Glycan Cluster Shielding and Antibody Epitopes on Lassa Virus Envelop Protein

Suyong Re[1, 2,*] and Kenji Mizuguchi[1, 3, 4,*]

[1]Center for Drug Design Research, National Institutes of Biomedical Innovation, Health, and Nutrition, 7-6-8 Saito-Asagi, Ibaraki, Osaka 567-0085 Japan

[2]RIKEN Center for Biosystems Dynamics Research, Integrated Innovation Building 7F, 6-7-1 Minatojima-minamimachi, Chuo-ku, Kobe, Hyogo 650-0047, Japan

[3]Artificial Intelligence Center for Health and Biomedical Research, National Institutes of Biomedical Innovation, Health, and Nutrition, 7-6-8 Saito-Asagi, Ibaraki, Osaka 567-0085 Japan

[4]Institute for Protein Research, Osaka University, 3-2 Yamadaoka, Suita, Osaka 565-0871, Japan

ABSTRACT: An understanding of how an antiviral monoclonal antibody recognizes its target is vital for the development of neutralizing antibodies and vaccines. The extensive glycosylation of viral proteins almost certainly affects the antibody response, but the investigation of such effects is hampered by the huge range of structures and interactions of surface glycans through their inherent complexity and flexibility. Here, we built an atomistic model of a fully glycosylated envelope protein complex of the Lassa virus and performed molecular dynamics simulations to characterize the impact of surface glycans on the antibody response. The simulations attested to the variety of conformations and interactions of surface glycans. The results show that glycosylation non-uniformly shields the surface of the complex, and only marginally affects protein dynamics. The glycans gather in distinct clusters through interaction with protein residues, and only a few regions are left accessible by an antibody. We successfully recovered known protein epitopes by integrating the simulation results with existing sequence- and structure-based epitope prediction methods. The results emphasize the rich structural environment of glycans and demonstrate that shielding is not merely envelopment by a

uniform blanket of sugars. This work provides a molecular basis for integrating otherwise elusive structural properties of glycans into vaccine and neutralizing antibody developments.

*Corresponding Authors: suyongre@nibiohn.go.jp, kenji@nibiohn.go.jp

Introduction

Glycosylation of proteins is an ubiquitous biomolecular process whereby carbohydrates or chains of carbohydrates are covalently attached to proteins. It adds extra functions or modulates existing functions of proteins, thereby affecting a range of cellular processes and diseases. Many viral proteins, such as those of HIV and the corona viruses, are extensively glycosylated.[1] The glycans on the surface of a viral envelope protein can facilitate infection by either interfering with the antibody response or aiding interaction with host cell proteins, though functional mechanisms at the molecular level remain largely unknown.

Lassa virus (LASV) is an arenaviruses resulting in hemorrhagic fever and causes up to 5000 deaths in West African endemic countries every year.[2] While there are no approved LASV vaccines yet, the study of the components and architecture of LASV relevant to infection is ongoing.[3–11] The sole antigen at the surface of the virus is a glycoprotein complex (GPC) which is a trimer of a two-subunit heterodimer consisting of a receptor binding subunit (GP1) and a transmembrane fusion-mediating subunit (GP2) (Figure 1a). There are 11 glycosylation sites on each of the protomers, GP1 and GP2, which are largely occupied by oligomannose-type (high mannose-type) N-glycans.[12] An X-ray crystal structure of GPC complexed with a neutralizing antibody (PDBID: 5VK2), while missing much of the glycan coordinates, suggests that the "glycan shield" is quite comprehensive and only a few regions are left accessible for antibody binding.[7] A study of 113 human monoclonal antibodies against LASV found that most of the antibodies bind to an assembled GPC but not to GP1 or GP2 alone.[13] Envelope glycans slow the binding rate of antibodies in mice.[14] While the impact of glycans on the antibody response is not in doubt, the structural complexity and high flexibility of glycans make molecular characterization extremely difficult.

Molecular dynamics (MD) simulations provide atomistic structure information, incorporating dynamics, for complex biomolecules. The structure ensembles from the simulation can be used to characterize structures/motions of flexible biomolecules relevant to the function of glycans, which are difficult to obtain from experiments. Recently, successful applications of MD simulation to the

SARS-CoV-2 corona virus have revealed in atomic detail both the protective and the passive roles of the "glycan shield" of the spike proteins in infection.[15–17] The known epitopes of the virus were successfully identified,[15] thereby showing the potential of MD simulations.

In this work, we characterize the "glycan shield" and the antibody response of LASV GPC using MD simulations. LASV exhibits dense glycosylation (shielding density of ~15% compared to 5% of SARS) and a higher proportion of oligomannose-type glycans (50% compared to ~30% of SARS).[1,18] These features raise the possibilities of a more effective "glycan shield" with respect to epitopes for antibody recognition, and its effect on protein dynamics. The work on HIV revealed the presence of distinct glycan clusters ("mannose patch") which may have a bearing on function.[12,19–23] Here we build an atomistic model of a fully glycosylated LASV GPC followed by micro-second scale MD simulations. We demonstrate that the glycans indeed form distinct clusters while only marginally affecting protein dynamics. By following the recent approach taken for SARS-CoV-2 epitope prediction,[15] the simulation results are integrated with sequence- and structure-based epitope prediction methods, enabling us to recover experimentally known epitopes. LASV is currently classified at biosafety level of 4 (BLS-4), which requires the highest level of precautions and limits experimental studies. This work, together with well-established *in-silico* epitope predictions,[24,25] could help design anti-viral vaccines and neutralizing antibodies with glycosylation effects in atomistic detail.

Methods

Simulation models. MD simulations were performed on three models of LASV GPC: one without glycans and two with 11 glycans in each monomer consisting of either only oligomannose-type ($Man_9GlcNAc_2$) or a mixture of oligomannose, complex, and hybrid-type N-glycans. For the mixture model, the glycan at each site was determined according to the experimentally derived glycoform[12] (the most dominant glycoform at each site was selected) (Figures 1a and S1 of Supporting Information). For all models, the X-ray crystal structure of a prefusion ectodomain LASV GPC bound

to a neutralizing antibody (PDBID: 5VK2)[7] was used as an initial configuration. CHARMM-GUI Glycan Modeler[26] was used to add glycans and construct simulation boxes. Each monomer in the models includes GP1 (residue index of 59–255) and GP2 (residue index of 260–416) subunits. The missing residues in the crystal structures were complemented using GALAXY modeling tool.[27] Asp311, Asp357, and Glu404 were protonated according to the pKa values (~7 at least in one of three monomers) estimated from PROPKA3.[28] Each system was finally solvated in 150 mM KCl solution (e.g. 240 K^+, 222 Cl^-, and 78,582 water molecules with a box dimension of 137 $Å^3$ for the mixture model after an equilibration).

MD simulations. All simulations were performed using the GENESIS program package (version 1.4.0).[29,30] We used CHARMM36m force field[31–33] and TIP3P[34] parameters for the glycoprotein and water molecules, respectively. All bonds involving hydrogen atoms were constrained using the SHAKE algrithm[35], while water molecules were kept rigid using the SETTLE algorithm[36]. Long-range electrostatic interactions were evaluated using Particle-mesh Ewald summation (PME).[37,38] For non-bonded interactions, force-switching function[39] was used to smoothly switch off the interaction at a range of 10 – 12 Å. A time step of 2.5 fs was used with r-RESPA integrator[40], where PME calculation was performed every 2 steps. All simulations were performed in an NPT ensemble at standard condition (300 K, 1 atm) using Bussi thermostat and barostat.[41,42] Each model was minimized first, and gradually heated up to 300 K and equilibrated for 100 ns, followed by 1 μs of production simulation. One microsecond may be short, but the conformations of both protein and glycans were sufficiently converged for the analysis (Figure S2 of Supporting Information).

Analysis of the simulation trajectory. Given that the LASV GPC is a trimer of heterodimer (GP1 and GP2), the analyses were performed for each of three protomers followed by averaging. This increases the number of sampled conformations in the analyses (1 μs × 3), improving statistical accuracy. Only the glycan-glycan contact analysis was performed over the trimer complex. The

structures for the analyses were collected every 10 ns (100 snapshots in total), except for the root mean square fluctuation (RMSF) calculation that uses all 100,000 snapshots.

Solvent Accessible Surface Area (SASA). SASA values were obtained using *measure sasa* function in VMD.[43,44] The *restrict* option, which considers only solvent accessible points near the user specified region, was used to calculate SASA values either per domain or per residue. SASA values were calculated using a range of probe radii (2 Å ~ 15 Å), including the typical value of 1.4 Å (a sphere of water), to examine accessibility of molecules with different sizes.[16] The particular value of 7.2 Å, which approximates the hypervariable loops of anti-gp120 antibodies,[17] was also used to infer the accessible area to antibodies.

Glycan-glycan and per residue interaction analysis. Glycan-glycan interaction was evaluated by counting the number of contacts between any heavy atoms of a glycan and those of other glycans using the *measure contact* function in VMD[43] with a cutoff distance of 5 Å. The value for each interaction pair was normalized for the total number of contacts. Similarly, a per residue interaction pattern (the interaction between a given residue and surroundings including other protein residues, glycans, and water molecules) was evaluated for all GP1 and GP2 residues (residues 59-416).

PyMOL software[45] was used for generating the images of the molecular structures.

Epitope prediction. Epitope probability was predicted using publicly available online servers: BepiPred 2.0[46] (http://www.cbs.dtu.dk/services/BepiPred/) for sequence-based prediction and Ellipro[47] (http://tools.iedb.org/ellipro/) for structure-based prediction, respectively. Default settings were used for both predictions (Epitope Threshold of 0.5 in BepiPred and Minimum score of 0.5 and Maximum distance of 6 Å in Ellipro). The input sequence in Fasta format for BepiPred was obtained from UniProt server (https://www.uniprot.org) (Entry: P08669). The crystal structure of LASV GPC (PDBID: 5VK2)[7] with missing residues complemented was used as an input for Ellipro and only one of the monomers (chain A (GP1) and chain a (GP2) in the original PDB structure) was selected for predictions.

Consensus epitope score. We integrated simulation results with sequence- and structure-based epitope predictions similar to the method of Sikora and coworkers for SARS-CoV-2.[15] We used the inverse of RMSF, a per residue SASA (probe radius of 7.2 Å), and the per residue contact with water molecules from the simulations. All values, including per residue epitope probabilities from BepiPred and Ellipro, were scaled to fit a 0 to 1 range. The per residue SASA and the per residue contact with water molecules both represent the degree of protein exposure to solvent, but the latter provides finer information on atomistic interactions, thus they were combined with arbitrary weight factors. The following equation was used to obtain our consensus score which was also scaled to fit in a range of 0 to 1.

$$S = S_{BipePred} \times S_{Ellipro} \times S_{1/RMSF} \times (0.75 \times S_{SASA} + 0.25 \times S_{Contact})$$

Results

Structure of GPC trimer and known epitopes. The modeled structure of glycosylated GPC trimer (mixture model) is shown in Figures 1b and 1c. There are seven and four glycans attached to GP1 (colored in yellow) and GP2 (colored in light blue), respectively. In all, 33 glycans densely shield the trimer surface particularly at its side and lower portions. The location of putative antibody epitopes, which were derived from an extensive analysis of memory B cell-origin 113 LASV specific monoclonal antibodies,[13] are also shown in Figure 1d. Many of these are located on the GP2 surface (the lower part of trimer). In what follows, we mainly describe and discuss the results of the mixture model unless otherwise specifically noted.

Effect of glycans on protein motion. We first examine the effect of the glycan shield on the protein motions. Figure 2 shows the Cα atoms root mean-square fluctuations (RMSFs) of GPC trimers with and without glycans. Overall, the features of the RMSFs do not change with or without attached glycans. There are two large peaks centered at Gly174 and Lys272, which originate from interface loop regions between different monomers. The loop region around Gly174 located in the upper part

of the trimer is invisible in the crystal structure (PDBID: 5VK2). The region around Lys272 is located just before the fusion loop in GP2. Two minor peaks around Ala202 and Gly391 for the GPC glycans are noticeably reduced by glycosylation. The Gly391 locates near $N390_{GP2}$ and $N395_{GP2}$ glycans, suggesting rigidification by direct contact with these glycans. The same mechanism is likely applicable to the Ala202, which locates near the Gly391 in the three-dimensional structure although they are far apart along the sequence.

Glycans shielding of GP1 and GP2. We next examine the extent of glycan shielding. The solvent accessible surface area (SASA) provides a useful measure of the extent of shielding.[16] We calculated SASA values for each of the GP1 and GP2 subunits with and without glycans. The extent of glycan shielding was then calculated by subtracting the SASA value with glycan from that without glycan and taking a ratio over the latter. The larger the obtained value, the larger the glycan shielding. The values were calculated using a range of probe radii from 1.4 Å, a typical value corresponding to a sphere of water, to 15 Å.[16] As shown in Figure 3, GP1 is more significantly shielded by glycans than GP2, where the extent of shielding reaches 47% for the probe radius of 15 Å. This non-uniform shielding is also illustrated in a collective view of ten snapshots (every 100 ns) from the simulation (Figure 3). We also calculated SASA values for each residue (per residue SASA with a probe radius of 7.2 Å representing the hypervariable loops of antibodies[17]) and mapped them on the monomer structure, showing that glycan shielding leaves only a few portions, mainly in GP2, accessible to antibody binding. The difference in the shielding between GP1 and GP2 increases with probe radius, suggesting that GP1 becomes more inaccessible for binding antibody with increasing molecular size of the partner.

Glycan-glycan interactions and clusters. The presence of a high level of under-processed oligomannose-type N-glycans is a feature of virus envelope proteins.[1,48] The structural study of LASV GPC[12] suggests that these oligomannose-type N-glycans form a cluster, as reported for HIV-1.[12,19–23]

To examine potential cluster formation, we calculated the probability of finding close glycan-glycan contacts in which the distance between any heavy atoms of a pair of glycans is less than 5 Å during the simulation. In Figure 4a, a contact map representation of the glycan-glycan interactions shows distinct intra-monomer interaction pairs involving $N79_{GP1}$, $N99_{GP1}$, $N109_{GP1}$, $N167_{GP1}$, $N365_{GP2}$, $N390_{GP2}$, and $N395_{GP2}$. In addition, there is an inter-monomer interaction pair involving $N119_{GP1}$. A typical snapshot from the simulation illustrates that these glycans form distinct clusters spanning GP1 and GP2 subunits (Figure 4b). Note that the clusters consist of either the under-processed oligomannose-type glycans ($N79_{GP1}$ and $N99_{GP1}$) or a mixture of three types (oligomannose, hybrid, and complex-types). The major and minor intra-monomer clusters, which involve $N109_{GP1}$, $N167_{GP1}$, $N365_{GP2}$, $N390_{GP2}$, and $N395_{GP2}$ for the former and $N79_{GP1}$, $N99_{GP1}$ for the latter, shield opposite side of the monomer. On the other hand, the cluster consisting of $N119_{GP1}$ shields the upper part of the monomer. This inter-monomer cluster occludes the binding site residues (His141, Asn146, Phe147, and Tyr150) toward α-dystroglycan (α-DG) relevant for host cell entry,[49] consistent with the experimental results that mutation of N119 increases an antibody response[14] and inhibits proteolytic processing.[50] The intra-monomer clusters do not involve $N89_{GP1}$ which was thought to be a member of the oligomannose cluster.[12] Our result instead shows that $N89_{GP1}$ spans the space left by two intra-monomer clusters and occludes the binding site (histidine triad: His92, His93, and His230) for lysosomal-associated membrane protein 1 (LAMP1) related to GP1 dissociation.

Glycan-protein interactions. To further quantify the effect of glycans on protein interactions, we determined the interaction pattern of each residue of both GP1 and GP2 with surroundings, that is with other residues of either the same monomer or different ones, with glycans, and with water molecules (Figure 5). The interactions of each residue were obtained by counting the number of contacts between any heavy atoms of the residue and those of each interaction partner with a distance cutoff of 5 Å. In Figure 5, the positions of functional regions and known epitopes are also shown for comparison. There are three classes of interaction patterns representing the local environment of GPC

residues. The interactions with the same monomer (grey bar in Figure 5a) and with water molecules (blue bar) respectively dominate the buried and solvent exposed residues, while both intra- and inter-monomer interactions (grey and orange bars) are prominent for interface residues. Note that the solvent-exposed regions overlap with many known epitopes (Figures 5a and 5b). While the glycans interact with residues in each of three regions to a varying extent, we highlight two types of glycan-protein interactions relevant for an antibody response. Firstly, the solvent-exposed residues, 114-119 (in α1 helix in GP1) and 388-395 (between GP2 T-loop and HR2), show substantial interaction with glycans, experiencing local shielding. The former interacts with glycans at $N119_{GP1}$ and $N167_{GP1}$ (Figure 5c), while the latter with those at $N365_{GP2}$, $N390_{GP2}$, and $N395_{GP2}$ (Figure 5d). The result is consistent with the recent experimental finding that $N390_{GP2}$ and $N395_{GP2}$ diminish antibody neutralization potency.[5] The second feature is the glycan interaction with interface residues 323-331 (in HR1 region of GP2). Our analysis identifies several interface residues critical for trimer formation (large orange bar in Figure 5a), including Ser138, mutation of which prevented the rescue of a recombinant viron.[6,7] Similarly, Arg325 and Leu326 show significant inter-monomer interactions. Two glycans, $N79_{GP1}$ and $N99_{GP1}$, interact with neighbors of these residues, likely stabilizing the interface (Figure 5e). These features signify that certain glycans either shield protein residues locally or stabilize the interface between monomers.

Effect of glycoform. The surface glycans could take several different forms (different types and various combinations of saccharides: "glycoform"). How sensitive glycan shielding is to glycoforms is an open question. A recent structural study on glycoforms of SARS-CoV-2 suggests sensitivity is minimal.[17] We compare the aforementioned glycan shielding of the mixture model with that of an oligomannose model, where 11 glycosylation sites are occupied solely by an oligomannose-type N-glycan ($Man_9GlcNAc_2$). We find qualitatively the same trend for both models (Figures S3-S6 of Supporting Information). In the oligomannose model the extent of GP2 shielding is greater, while that of GP1 shows more variation among monomers particularly with larger probes (Figure S4 of

Supporting Information). Analysis of glycan-glycan interactions shows that the oligomannose model predisposes to extra inter-monomer interactions involving GP2-attached glycans (Figure S5 of Supporting Information), whereas protein-glycan interactions remain the same qualitatively (Figure S6 of Supporting Information). This examination, although crude, suggests that glycan shielding is wider and more labile before glycan processing or maturation by enzymes. The changess are quantitative and likely hold regardless of glycoforms.

Epitope prediction. Finally, we predict potential epitopes taking glycan shielding into account. Identification of epitopes is essential for the development of vaccines and neutralizing antibodies and several computational methods have been developed for epitope prediction. BepiPred is a sequence-based epitope prediction method which uses a random forest algorithm trained on epitopes annotated from antibody-antigen protein structures.[46] On the other hand, ElliPro, which is a structure-based method, uses antigenicity, solvent accessibility, and flexibility of protein structures.[47] These methods are powerful and fast approaches to epitope identification, but do not take glycan effects into account. To overcome this limitation, we combine our simulation results on glycan shielding with these methods. We follow the approach taken by Sikora and co-workers for SASRS-CoV-2 spike epitopes, where the effect of a glycan shield was represented by the rigidity and accessibility of protein residues.[15] The present work uses the RMSF, SASA, and the interaction with water solvent to estimate the shielding effect on each protein residue. Given that rigid and accessible regions present potential epitopes, we set the scores higher the smaller the RMSF with both SASA and the interaction larger. Figure 6a summarizes the epitope probabilities from BepiPred and ElliPro, RMSF, SASA, and interaction scores, and the consensus score. While BepiPred and ElliPro predict many potential regions, glycan shielding effectively leaves only a few regions as potential epitope candidates (Figures 6a and 6b). As more sophisticated preceding works,[15,24] we are able to recover just about all experimentally known epitopes, demonstrating the potential of this approach. Two of the known epitopes (GPC-A: residues 272-285 and GPC-B: residues 361-375) have low prediction scores. These

epitopes correspond to surface loops near the interfaces between intra-protomer subunits or different protomers, and are partly occluded by glycans. Other conformations, not sampled by the current simulation, may produce better scores. The low scores are also likely due to the choice of parameter used in the SASA calculation (probe radius of 7.2 Å). Regions partly shielded by glycans are inaccessible to large molecules, but a flexible loop of antibodies may reach them. Further tuning of the parameter should improve the prediction results. In addition to the known epitopes, we predict a few other candidate epitopes. For example, the residues following η4 from GP1 (residues 205-210) bind to human neutralizing antibody Fab 37.7H as shown in a collective view of 10 snapshots from the simulation aligned to the crystal structure (PDBID: 5VK2) (Figure 6c). The antibody binding to these residues together with the known epitopes for GPC-A/B antibodies is consistent with the finding that most antibody bindings require an assembled GPC.[13] Note that four glycans ($N79_{GP1}$, $N99_{GP1}$, $N390_{GP2}$, and $N395_{GP2}$) nicely coordinate Fab 37.7H. Though $N390_{GP2}$ and $N395_{GP2}$ locally shield the binding region to the antibody, it seems they contribute to stabilize antibody binding: the de-shielding cost is offset by the gain through binding.

Discussion and Conclusions

The concept of glycan shielding, while not new, is gaining increasing support.[1,51] Recently, it has attracted attention and become a hot topic through the rapid exploration of structures of the SARS-CoV-2 spike protein.[15–18] Advances in both experimental techniques and MD simulations now enable us to analyze glycan shielding at atomic resolution.[52,53] Our results, together with previous simulations on SARS-CoV-2 spike proteins,[15–17] illustrate the diversity of glycan shielding, encompassing a variety of structures and interactions. The glycans provide protection through a rich structural environment – not just shielding by a uniform blanket. Our simulations of LASV GPC suggest surface N-glycans exist in distinct clusters. Clusters of oligomannose-type N-glycans, “mannose-patch”, are well characterized for HIV envelope proteins and have been shown to be a target for broadly neutralizing antibodies.[12,19–23] The clusters in LASV GPC, such as the one of oligomannose-type

glycans $N79_{GP1}$ and $N79_{GP1}$, likely also serve as targets for antibody binding. There are antibodies that bind to complex-type glycans,[54,55] and they may target the observed clusters made of a mixture of oligomannose, hybrid, and complex-type glycans. We also show that certain glycans, such as $N365_{GP2}$, $N390_{GP2}$, and $N395_{GP2}$, directly interact with otherwise solvent-exposed GPC residues to locally mask them. In fact, site-selective deglycosylation targeting these glycans improves immunogenicity.[14,56] Intriguingly, these glycans belong to one of the clusters observed in this study. Cluster formation appears to facilitate the shielding of specific regions by concentrating certain glycans at otherwise critical positions.

The MD simulation captures important features of glycan shielding, but how these change over a longer time scale requires further elucidation. Conformational changes in N-glycans in general require surmounting high-energy barriers associated with glycosidic linkages, involving costly functional group rotations and rearrangements of hydrogen bond networks. Conventional MD simulations of glycans tend to become trapped in one of the local minima, sampling only limited conformational space. Enhanced-sampling methods potentially address the issues of the lifetime of distinct clusters and the existence of other clusters.[53] Previously, we applied the replica-exchange molecular dynamics (REMD) method,[57] which effectively overcomes the high energy barriers needed to sample a wider conformational space, to characterize the conformational ensemble of a N-glycan in solution,[58,59] but extending such an approach to a heavily glycosylated protein remains challenging. Computationally less demanding methods, such as a combined replica state exchange with metadynamics (RSE-MTD),[60,61] replica exchange with solute tempering (REST),[62–65] and Gaussian accelerated MD (GaMD)[66] may be useful.[67]

Epitope prediction is extremely valuable for designing vaccines and antibodies. Computational approaches, encompassed in the field of immunoinformatics, are evolving into an essential tool for facilitating the identification of epitopes, and are now widely applied to predict viral, bacterial and

tumoral epitopes of B and T cells.[68] Given that both antigens and antibodies are often heavily glycosylated, it is pertinent to take into account the effect of glycans. By combining MD simulations with immunoinformatics we are able to not only improve the accuracy of epitope prediction but also elucidate a complex structure of an envelope protein with associated glycans. This study could be extended to the development of molecular models of complex antigen-antibody interactions with details of explicit glycan involvement.

Associated Content

Supporting Information

The Supporting Information is available free of charge on the ACS Publications website. Additional Figures S1－S6 (PDF)

Author Information

Corresponding Authors

Suyong Re – Center for Drug Design Research, National Institutes of Biomedical Innovation, Health, and Nutrition, 7-6-8 Saito-Asagi, Ibaraki, Osaka 567-0085 Japan, RIKEN Center for Biosystems Dynamics Research, Integrated Innovation Building 7F, 6-7-1 Minatojima-minamimachi, Chuo-ku, Kobe, Hyogo 650-0047, Japan; orcid.org/0000-0002-3752-6554

Email: suyongre@nibiohn.go.jp

Kenji Mizuguchi – Artificial Intelligence Center for Health and Biomedical Research, National Institutes of Biomedical Innovation, Health, and Nutrition, 7-6-8 Saito-Asagi, Ibaraki, Osaka 567-0085 Japan; Institute for Protein Research, Osaka University, 3-2 Yamadaoka, Suita, Osaka 565-0871, Japan; orcid.org/0000-0003-3021-7078

Email: kenji@nibiohn.go.jp

Notes

The authors declare no competing financial interest.

Acknowledgments

We thank Dr. Yuji Sugita for his scientific advices and comments on the manuscript, and Dr. David McIntosh for his critical reading of the manuscript. The computations were performed using Research Center for Computational Science (Okazaki, Japan) as well as the computational resources in RIKEN Biosystems Dynamics Research (Kobe, Japan) and in National Institutes of Biomedical Innovation, Health and Nutrition (Osaka Japan). This research was supported by MEXT/JSPS KAKENHI Grant Number 19K12229 (to S.R.).

References

(1) Watanabe, Y.; Bowden, T. A.; Wilson, I. A.; Crispin, M. Exploitation of Glycosylation in Enveloped Virus Pathobiology. *Biochim. Biophys. Acta - Gen. Subj.* **2019**, *1863*, 1480–1497.

(2) World Health Organization. Lassa Fever Research and Development Roadmap. **2018**, No. May, 1–18.

(3) Ibukun, F. I. Inter-Lineage Variation of Lassa Virus Glycoprotein Epitopes: A Challenge to Lassa Virus Vaccine Development. *Viruses* **2020**, *12*, 386.

(4) Crispin, M.; Zeltina, A.; Zitzmann, N.; Bowden, T. A. Native Functionality and Therapeutic Targeting of Arenaviral Glycoproteins. *Curr. Opin. Virol.* **2016**, *18*, 70–75.

(5) Hastie, K. M.; Cross, R. W.; Harkins, S. S.; Zandonatti, M. A.; Koval, A. P.; Heinrich, M. L.; Rowland, M. M.; Robinson, J. E.; Geisbert, T. W.; Garry, R. F. et al. Convergent Structures Illuminate Features for Germline Antibody Binding and Pan-Lassa Virus Neutralization. *Cell* **2019**, *178*, 1004-1015.e14.

(6) Hastie, K. M.; Igonet, S.; Sullivan, B. M.; Legrand, P.; Zandonatti, M. A.; Robinson, J. E.; Garry, R. F.; Rey, F. A.; Oldstone, M. B.; Saphire, E. O. Crystal Structure of the Prefusion Surface Glycoprotein of the Prototypic Arenavirus LCMV. *Nat. Struct. Mol. Biol.* **2016**, *23*, 513–521.

(7) Hastie, K. M.; Zandonatti, M. A.; Kleinfelter, L. M.; Heinrich, M. L.; Rowland, M. M.;

Chandran, K.; Branco, L. M.; Robinson, J. E.; Garry, R. F.; Saphire, E. O. Structural Basis for Antibody-Mediated Neutralization of Lassa Virus. *Science* **2017**, *356*, 923–928.

(8) Li, S.; Sun, Z.; Pryce, R.; Parsy, M. L.; Fehling, S. K.; Schlie, K.; Siebert, C. A.; Garten, W.; Bowden, T. A.; Strecker, T. et al. Acidic PH-Induced Conformations and LAMP1 Binding of the Lassa Virus Glycoprotein Spike. *PLoS Pathog.* **2016**, *12*, e1005418.

(9) Zeltina, A.; Bowden, T. A. Human Antibody Pieces Together the Puzzle of the Trimeric Lassa Virus Surface Antigen. *Nat. Struct. Mol. Biol.* **2017**, *24*, 559–560.

(10) Jae, L. T.; Raaben, M.; Herbert, A. S.; Kuehne, A. I.; Wirchnianski, A. S.; Soh, T. K.; Stubbs, S. H.; Janssen, H.; Damme, M.; Saftig, P. et al. Lassa Virus Entry Requires a Trigger-Induced Receptor Switch. *Science* **2014**, *344*, 1506–1510.

(11) Torriani, G.; Galan-Navarro, C.; Kunz, S. Lassa Virus Cell Entry Reveals New Aspects of Virus-Host Cell Interaction. *J. Virol.* **2017**, *91*, 1–8.

(12) Watanabe, Y.; Raghwani, J.; Allen, J. D.; Seabright, G. E.; Li, S.; Moser, F.; Huiskonen, J. T.; Strecker, T.; Bowden, T. A.; Crispin, M. Structure of the Lassa Virus Glycan Shield Provides a Model for Immunological Resistance. *Proc. Natl. Acad. Sci. U. S. A.* **2018**, *115*, 7320–7325.

(13) Robinson, J. E.; Hastie, K. M.; Cross, R. W.; Yenni, R. E.; Elliott, D. H.; Rouelle, J. A.; Kannadka, C. B.; Smira, A. A.; Garry, C. E.; Bradley, B. T. et al. Most Neutralizing Human Monoclonal Antibodies Target Novel Epitopes Requiring Both Lassa Virus Glycoprotein Subunits. *Nat. Commun.* **2016**, *7*, 11544.

(14) Sommerstein, R.; Flatz, L.; Remy, M. M.; Malinge, P.; Magistrelli, G.; Fischer, N.; Sahin, M.; Bergthaler, A.; Igonet, S.; ter Meulen, J. et al. Arenavirus Glycan Shield Promotes Neutralizing Antibody Evasion and Protracted Infection. *PLoS Pathog.* **2015**, *11*, e1005276.

(15) Sikora, M.; von Bülow, S.; Blanc, F. E. C.; Gecht, M.; Covino, R.; Hummer, G. Map of SARS-CoV-2 Spike Epitopes Not Shielded by Glycans. *bioRxiv* **2020**.

(16) Casalino, L.; Gaieb, Z.; Goldsmith, J. A.; Hjorth, C. K.; Dommer, A. C.; Harbison, A. M.; Fogarty, C. A.; Barros, E. P.; Taylor, B. C.; Mclellan, J. S. et al. Beyond Shielding: The Roles of Glycans in the SARS-CoV-2 Spike Protein. *ACS Cent. Sci.* **2020**, *6*, 1722–1734.

(17) Grant, O. C.; Montgomery, D.; Ito, K.; Woods, R. J. Analysis of the SARS-CoV-2 Spike Protein Glycan Shield Reveals Implications for Immune Recognition. *Sci. Rep.* **2020**, *10*, 1–

18.

(18) Watanabe, Y.; Berndsen, Z. T.; Raghwani, J.; Seabright, G. E.; Allen, J. D.; Pybus, O. G.; McLellan, J. S.; Wilson, I. A.; Bowden, T. A.; Ward, A. B. et al. Vulnerabilities in Coronavirus Glycan Shields despite Extensive Glycosylation. *Nat. Commun.* **2020**, *11*, 2688.

(19) Pritchard, L. K.; Spencer, D. I. R.; Royle, L.; Bonomelli, C.; Seabright, G. E.; Behrens, A. J.; Kulp, D. W.; Menis, S.; Krumm, S. A.; Dunlop, D. C. et al. Glycan Clustering Stabilizes the Mannose Patch of HIV-1 and Preserves Vulnerability to Broadly Neutralizing Antibodies. *Nat. Commun.* **2015**, *6*, 1–11.

(20) Behrens, A. J.; Vasiljevic, S.; Pritchard, L. K.; Harvey, D. J.; Andev, R. S.; Krumm, S. A.; Struwe, W. B.; Cupo, A.; Kumar, A.; Zitzmann, N. et al. Composition and Antigenic Effects of Individual Glycan Sites of a Trimeric HIV-1 Envelope Glycoprotein. *Cell Rep.* **2016**, *14*, 2695–2706.

(21) Coss, K. P.; Vasiljevic, S.; Pritchard, L. K.; Krumm, S. A.; Glaze, M.; Madzorera, S.; Moore, P. L.; Crispin, M.; Doores, K. J. HIV-1 Glycan Density Drives the Persistence of the Mannose Patch within an Infected Individual. *J. Virol.* **2016**, *90*, 11132–11144.

(22) Seabright, G. E.; Cottrell, C. A.; van Gils, M. J.; D'addabbo, A.; Harvey, D. J.; Behrens, A. J.; Allen, J. D.; Watanabe, Y.; Maker, A.; Vasiljevic, S. et al. Networks of HIV-1 Envelope Glycans Maintain Antibody Epitopes in the Face of Glycan Additions and Deletions. *bioRxiv* **2020**, 2020.02.21.959981.

(23) Crispin, M.; Ward, A. B.; Wilson, I. A. Structure and Immune Recognition of the HIV Glycan Shield. *Annu. Rev. Biophys.* **2018**, *47*, 499–523.

(24) Baral, P.; Pavadai, E.; Gerstman, B. S.; Chapagain, P. P. In-Silico Identification of the Vaccine Candidate Epitopes against the Lassa Virus Hemorrhagic Fever. *Sci. Rep.* **2020**, *10*, 7667.

(25) Verma, S. K.; Yadav, S.; Kumar, A. In Silico Prediction of B- and T- Cell Epitope on Lassa Virus Proteins for Peptide Based Subunit Vaccine Design. *Adv. Biomed. Res.* **2015**, *4*, 201–201.

(26) Park, S. J.; Lee, J.; Qi, Y.; Kern, N. R.; Lee, H. S.; Jo, S.; Joung, I.; Joo, K.; Lee, J.; Im, W. CHARMM-GUI Glycan Modeler for Modeling and Simulation of Carbohydrates and Glycoconjugates. *Glycobiology* **2019**, *29*, 320–331.

(27) Ko, J.; Park, H.; Seok, C. GalaxyTBM: Template-Based Modeling by Building a Reliable Core and Refining Unreliable Local Regions. *BMC Bioinformatics* **2012**, *13*, 198.

(28) Olsson, M. H. M.; SØndergaard, C. R.; Rostkowski, M.; Jensen, J. H. PROPKA3: Consistent Treatment of Internal and Surface Residues in Empirical p K a Predictions. *J. Chem. Theory Comput.* **2011**, *7*, 525–537.

(29) Kobayashi, C.; Jung, J.; Matsunaga, Y.; Mori, T.; Ando, T.; Tamura, K.; Kamiya, M.; Sugita, Y. GENESIS 1.1: A Hybrid-Parallel Molecular Dynamics Simulator with Enhanced Sampling Algorithms on Multiple Computational Platforms. *J. Comput. Chem.* **2017**, *38*, 2193–2206.

(30) Jung, J.; Mori, T.; Kobayashi, C.; Matsunaga, Y.; Yoda, T.; Feig, M.; Sugita, Y. GENESIS: A Hybrid-Parallel and Multi-Scale Molecular Dynamics Simulator with Enhanced Sampling Algorithms for Biomolecular and Cellular Simulations. *Wiley Interdiscip. Rev. Comput. Mol. Sci.* **2015**, *5*, 310–323.

(31) Huang, J.; Rauscher, S.; Nawrocki, G.; Ran, T.; Feig, M.; De Groot, B. L.; Grubmüller, H.; MacKerell, A. D. CHARMM36m: An Improved Force Field for Folded and Intrinsically Disordered Proteins. *Nat. Methods* **2016**, *14*, 71–73.

(32) Best, R. B.; Zhu, X.; Shim, J.; Lopes, P. E. M.; Mittal, J.; Feig, M.; MacKerell, A. D. Optimization of the Additive CHARMM All-Atom Protein Force Field Targeting Improved Sampling of the Backbone φ, ψ and Side-Chain X1 and X2 Dihedral Angles. *J. Chem. Theory Comput.* **2012**, *8*, 3257–3273.

(33) Guvench, O.; Greenr, S. N.; Kamath, G.; Brady, J. W.; Venable, R. M.; Pastor, R. W.; Mackerell, A. D. Additive Empirical Force Field for Hexopyranose Monosaccharides. *J. Comput. Chem.* **2008**, *29*, 2543–2564.

(34) Jorgensen, W. L.; Chandrasekhar, J.; Madura, J. D.; Impey, R. W.; Klein, M. L. Comparison of Simple Potential Functions for Simulating Liquid Water. *J. Chem. Phys.* **1983**, *79*, 926–935.

(35) Ryckaert, J. P.; Ciccotti, G.; Berendsen, H. J. C. Numerical Integration of the Cartesian Equations of Motion of a System with Constraints: Molecular Dynamics of n-Alkanes. *J. Comput. Phys.* **1977**, *23*, 327–341.

(36) Miyamoto, S.; Kollman, P. A. Settle: An Analytical Version of the SHAKE and RATTLE

Algorithm for Rigid Water Models. *J. Comput. Chem.* **1992**, *13*, 952–962.

(37) Essmann, U.; Perera, L.; Berkowitz, M. L.; Darden, T.; Lee, H.; Pedersen, L. G. A Smooth Particle Mesh Ewald Method. *J. Chem. Phys.* **1995**, *103*, 8577–8593.

(38) Darden, T.; York, D.; Pedersen, L. Particle Mesh Ewald: An N·log(N) Method for Ewald Sums in Large Systems. *J. Chem. Phys.* **1993**, *98*, 10089–10092.

(39) Steinbach, P. J.; Brooks, B. R. New Spherical-cutoff Methods for Long-range Forces in Macromolecular Simulation. *J. Comput. Chem.* **1994**, *15*, 667–683.

(40) Tuckerman, M.; Berne, B. J.; Martyna, G. J. Reversible Multiple Time Scale Molecular Dynamics. *J. Chem. Phys.* **1992**, *97*, 1990–2001.

(41) Bussi, G.; Donadio, D.; Parrinello, M. Canonical Sampling through Velocity Rescaling. *J. Chem. Phys.* **2007**, *126*, 014101.

(42) Bussi, G.; Zykova-Timan, T.; Parrinello, M. Isothermal-Isobaric Molecular Dynamics Using Stochastic Velocity Rescaling. *J. Chem. Phys.* **2009**, *130*, 074101.

(43) Humphrey, W.; Dalke, A.; Schulten, K. VMD: Visual Molecular Dynamics. *J. Mol. Graph.* **1996**, *14*, 33–38.

(44) Shrake, A.; Rupley, J. A. Environment and Exposure to Solvent of Protein Atoms. Lysozyme and Insulin. *J. Mol. Biol.* **1973**, *79*, 351–371.

(45) Delano, W. L. The PyMOL Molecular Graphics System. 2002.

(46) Jespersen, M. C.; Peters, B.; Nielsen, M.; Marcatili, P. BepiPred-2.0: Improving Sequence-Based B-Cell Epitope Prediction Using Conformational Epitopes. *Nucleic Acids Res.* **2017**, *45*, W24–W29.

(47) Ponomarenko, J.; Bui, H. H.; Li, W.; Fusseder, N.; Bourne, P. E.; Sette, A.; Peters, B. ElliPro: A New Structure-Based Tool for the Prediction of Antibody Epitopes. *BMC Bioinformatics* **2008**, *9*, 514.

(48) Doores, K. J.; Bonomelli, C.; Harvey, D. J.; Vasiljevic, S.; Dwek, R. A.; Burton, D. R.; Crispin, M.; Scanlan, C. N. Envelope Glycans of Immunodeficiency Virions Are Almost Entirely Oligomannose Antigens. *Proc. Natl. Acad. Sci. U. S. A.* **2010**, *107*, 13800–13805.

(49) Acciani, M.; Alston, J. T.; Zhao, G.; Reynolds, H.; Ali, A. M.; Xu, B.; Brindley, M. A. Mutational Analysis of Lassa Virus Glycoprotein Highlights Regions Required for Alpha-Dystroglycan Utilization. *J. Virol.* **2017**, *91*.

(50) Zhu, X.; Liu, Y.; Guo, J.; Wang, Z.; Cao, J.; Xiao, G.; Wang, W. Effects of N-Linked Glycan of Lassa Virus Envelope Glycoprotein on the Immune Response. *bioRxiv* **2020**, 2020.09.29.319855.

(51) Wei, X.; Decker, J. M.; Wang, S.; Hui, H.; Kappes, J. C.; Wu, X.; Salazar-Gonzalez, J. F.; Salazar, M. G.; Kilby, J. M.; Saag, M. S. et al. Antibody Neutralization and Escape by HIV-1. *Nature* **2003**, *422*, 307–312.

(52) Berndsen, Z. T.; Chakraborty, S.; Wang, X.; Cottrell, C. A.; Torres, J. L.; Diedrich, J. K.; López, C. A.; Yates, J. R.; van Gils, M. J.; Paulson, J. C. et al. Visualization of the HIV-1 Env Glycan Shield across Scales. *Proc. Natl. Acad. Sci. U. S. A.* **2020**, *117*, 28014–28025.

(53) Yang, M.; Huang, J.; Simon, R.; Wang, L. X.; MacKerell, A. D. Conformational Heterogeneity of the HIV Envelope Glycan Shield. *Sci. Rep.* **2017**, *7*, 4435.

(54) Falkowska, E.; Le, K. M.; Ramos, A.; Doores, K. J.; Lee, J. H.; Blattner, C.; Ramirez, A.; Derking, R.; vanGils, M. J.; Liang, C. H. et al. Broadly Neutralizing HIV Antibodies Define a Glycan-Dependent Epitope on the Prefusion Conformation of Gp41 on Cleaved Envelope Trimers. *Immunity* **2014**, *40*, 657–668.

(55) Blattner, C.; Lee, J. H.; Sliepen, K.; Derking, R.; Falkowska, E.; delaPeña, A. T.; Cupo, A.; Julien, J. P.; vanGils, M.; Lee, P. S. et al. Structural Delineation of a Quaternary, Cleavage-Dependent Epitope at the Gp41-Gp120 Interface on Intact HIV-1 Env Trimers. *Immunity* **2014**, *40*, 669–680.

(56) Dowling, W.; Thompson, E.; Badger, C.; Mellquist, J. L.; Garrison, A. R.; Smith, J. M.; Paragas, J.; Hogan, R. J.; Schmaljohn, C. Influences of Glycosylation on Antigenicity, Immunogenicity, and Protective Efficacy of Ebola Virus GP DNA Vaccines. *J. Virol.* **2007**, *81*, 1821–1837.

(57) Sugita, Y.; Okamoto, Y. Replica-Exchange Molecular Dynamics Method for Protein Folding. *Chem. Phys. Lett.* **1999**, *314*, 141–151.

(58) Nishima, W.; Miyashita, N.; Yamaguchi, Y.; Sugita, Y.; Re, S. Effect of Bisecting GlcNAc and Core Fucosylation on Conformational Properties of Biantennary Complex-Type N-Glycans in Solution. *J. Phys. Chem. B* **2012**, *116*, 8504–8512.

(59) Re, S.; Nishima, W.; Miyashita, N.; Sugita, Y. Conformational Flexibility of N-Glycans in Solution Studied by REMD Simulations. *Biophys. Rev.* **2012**, *4*, 179–187.

(60) Galvelis, R.; Re, S.; Sugita, Y. Enhanced Conformational Sampling of N-Glycans in Solution with Replica State Exchange Metadynamics. *J. Chem. Theory Comput.* **2017**, *13*, 1934–1942.

(61) Galvelis, R.; Sugita, Y. Replica State Exchange Metadynamics for Improving the Convergence of Free Energy Estimates. *J. Comput. Chem.* **2015**, *36*, 1446–1455.

(62) Kamiya, M.; Sugita, Y. Flexible Selection of the Solute Region in Replica Exchange with Solute Tempering: Application to Protein-Folding Simulations. *J. Chem. Phys.* **2018**, *149*, 072304.

(63) Liu, P.; Kim, B.; Friesner, R. A.; Berne, B. J. Replica Exchange with Solute Tempering: A Method for Sampling Biological Systems in Explicit Water. *Proc. Natl. Acad. Sci. U. S. A.* **2005**, *102*, 13749–13754.

(64) Wang, L.; Friesner, R. A.; Berne, B. J. Replica Exchange with Solute Scaling: A More Efficient Version of Replica Exchange with Solute Tempering (REST2). *J. Phys. Chem. B* **2011**, *115*, 9431–9438.

(65) Terakawa, T.; Kameda, T.; Takada, S. On Easy Implementation of a Variant of the Replica Exchange with Solute Tempering in GROMACS. *J. Comput. Chem.* **2011**, *32*, 1228–1234.

(66) Miao, Y.; Sinko, W.; Pierce, L.; Bucher, D.; Walker, R. C.; McCammon, J. A. Improved Reweighting of Accelerated Molecular Dynamics Simulations for Free Energy Calculation. *J. Chem. Theory Comput.* **2014**, *10*, 2677–2689.

(67) Sugita, Y.; Kamiya, M.; Oshima, H.; Re, S. Replica-Exchange Methods for Biomolecular Simulations. *Methods Mol. Biol.* **2019**, *2022*, 155–177.

(68) Raoufi, E.; Hemmati, M.; Eftekhari, S.; Khaksaran, K.; Mahmodi, Z.; Farajollahi, M. M.; Mohsenzadegan, M. Epitope Prediction by Novel Immunoinformatics Approach: A State-of-the-Art Review. *Int. J. Pept. Res. Ther.* **2020**, *26*, 1155–1163.

FIGURES

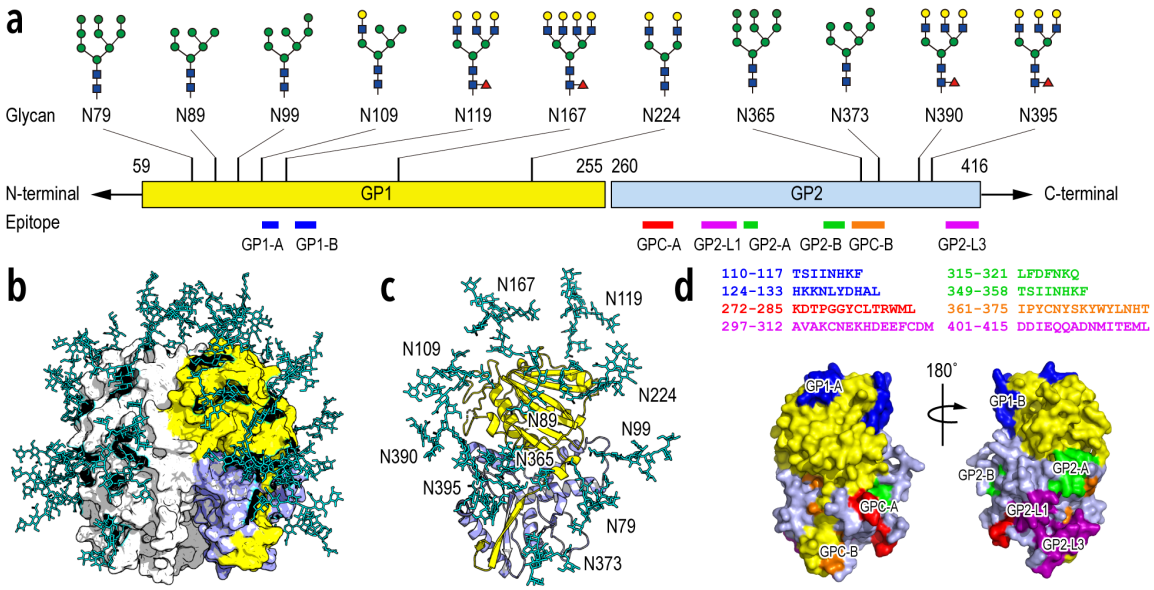

Figure 1. Structure model of GPC trimer and known epitopes. (a) Structures and positions of 11 N-glycans attached to each monomer (GP1/GP2 heterodimer) (b) Three-dimensional structure of the glycosylated GPC model (mixture model). Protein is shown with surface representation, while glycans with stick representation. GP1 and GP2 of a monomer are colored in yellow and light-blue, respectively. (c) Closeup view of the monomer. GP1 and GP2 are shown in cartoon representation in yellow and light-blue colors, respectively. (d) Location of putative epitopes derived from experiment (Ref. [13]) with their sequences. Epitopes are shown in different colors (blue: GP1-A/B, green: GP2-A/B, purple: GP2-L1/L3, red: GPC-A, and orange: GPC-B), while GP1 and GP2 outside the epitopes are colored in yellow and light-blue, respectively.

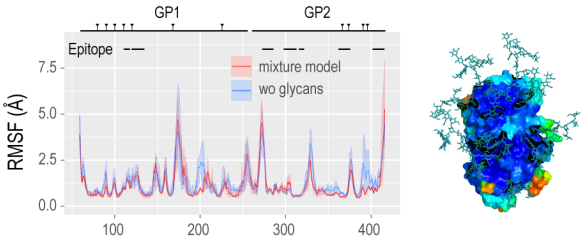

Figure 2. Protein fluctuation. Cα atoms root mean-square fluctuations (RMSFs) of GPC trimers with (red, mixture model) and without (blue) glycans. The corresponding color shades show the deviation of RMSF values in three monomers. The positions of the glycosylation sites (vertical bar with inverse triangle) and know epitopes (horizontal bar) are shown for comparison. The surface representation of the RMSF values averaged on three monomers (blue to red for 0.47 to 5.45 Å).

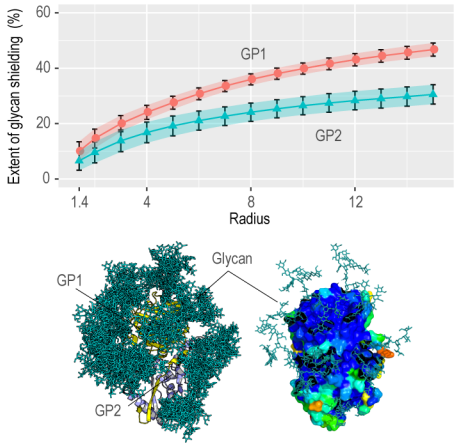

Figure 3. Glycan shielding. (Top) Extent of glycan shielding in each of the GP1 and GP2 domains estimated as a ratio of the reduction of solvent accessible surface area (SASA) upon glycosylation (mixture model) over SASA without glycans (($SASA_{wo/gly} - SASA_{wt/gly}$)/$SASA_{wo/gly} \times 100$)). The values are plotted along the probe radius used for SASA calculations. (Bottom) Molecular representation of the glycan shielding by an overlay of 10 frames (every 100 ns) of the simulation trajectory and the surface representation of per residue SASA values (blue to red for 0 to 549 $Å^2$).

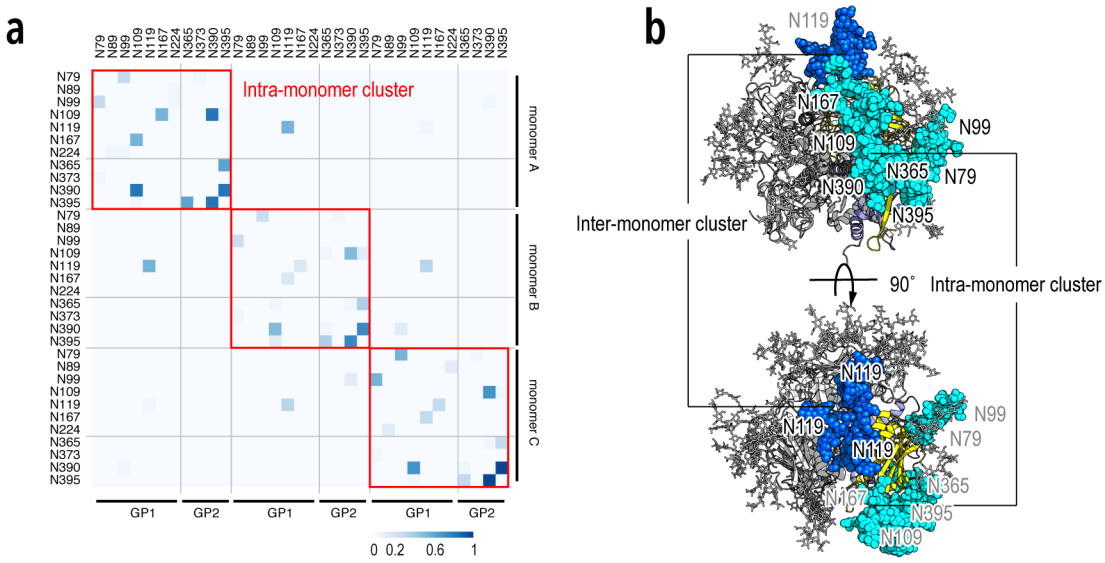

Figure 4. Glycan-glycan interaction. (a) A contact map representation of glycan-glycan interaction probability having the distance between any heavy atoms between a pair of glycans less than 5 Å in the simulation. Red box highlights the intra-monomer clusters. (b) A typical snapshot showing the intra- (cyan) and inter-monomer (blue) clusters.

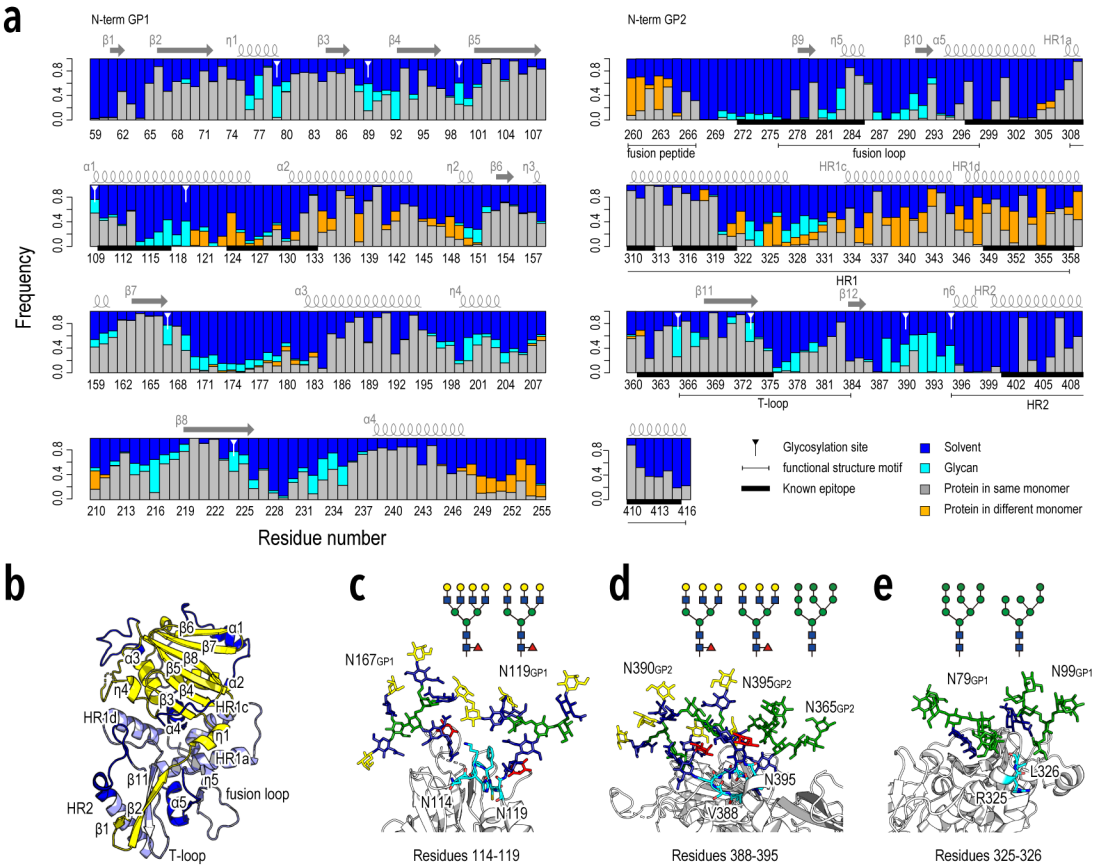

Figure 5. Glycan-protein interactions. (a) Interaction pattern of GPC residues of either GP1 (left) or GP2 (right) with their surroundings (other GPC residues, glycans, and water molecules). The interactions between a given residue and surroundings were calculated by counting the number of contacts in which the distance between any heavy atoms of an interaction pair is less than 5 Å. The numbers were normalized for each interaction partner to get relative frequency. For each residue, the interaction frequencies for different partners are shown (blue: water, cyan: glycans, gray: other residues in the same monomer, orange: other residues in the different monomer). The location of glycosylation sites, functional region, and known epitopes are also shown for comparison. (b) Major solvent-exposed regions (blue) mapped on the GPC monomer. (c-e) Typical snapshots showing the glycan-protein interactions. The protein residues interacting with glycans are colored in cyan. For glycans, the same color scheme as a simplified glycan representation is used.

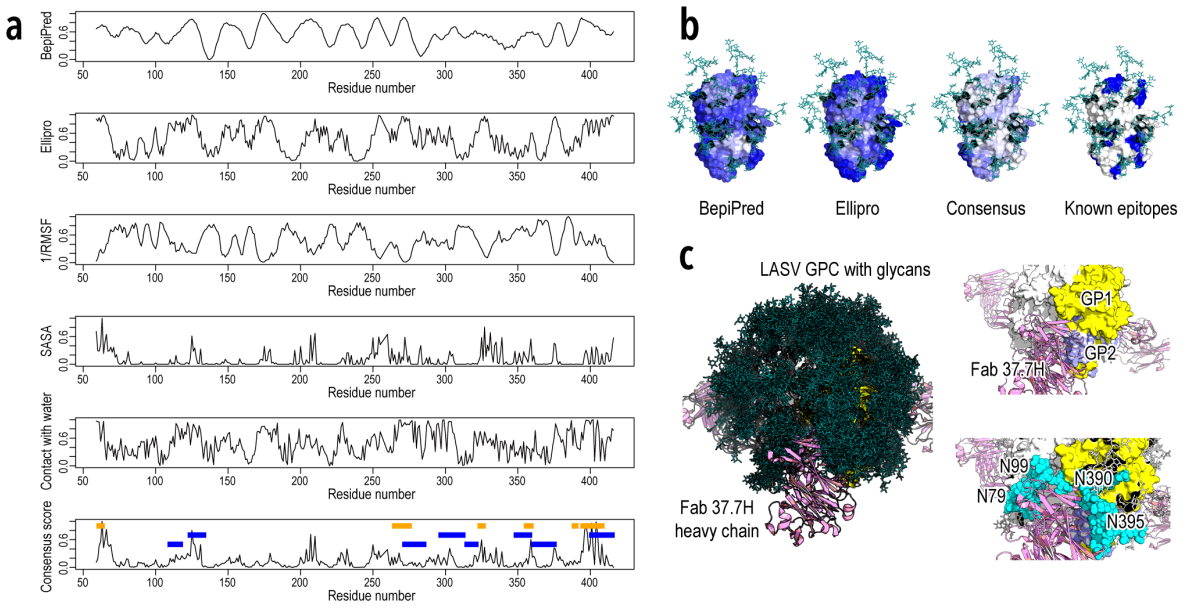

Figure 6. Predicted epitopes. (a) Consensus epitope score (bottom) and those of each component. All scores were scaled to have a range of values from 0 to 1. Positions of known epitopes and 37.7H epitope from the crystal structure (PDBID: 5vk2) are respectively marked as blue and orange bars for comparison. (b) Three epitope scores mapped on a GPC monomer structure (white to blue for 0 to 1). Know epitopes are also mapped on the same structure (blue). (c) A collection of 10 snapshots from the simulation aligned to the crystal structure with bound neutralized antibody and closeup views of binding region. GP1 and GP2 units are colored in yellow and light-blue, respectively. Two glycans, $N79_{GP1}$ and $N395_{GP2}$, are shown in sphere representation (cyan).

TOC Graphic